Geophys. Astrophys. Fluid Dynamics, Vol. 48, pp. 169–192
Reprints available directly from the publisher
Photocopying permitted by license only

INTERNAL HYDRAULIC CONTROL IN ROTATING FLUIDS—APPLICATIONS TO OCEANS

J. A. WHITEHEAD

Department of Physical Oceanography, Woods Hole Oceanographic Institution, Woods Hole, Massachusetts 02543, USA

(Received 11 January 1989; in final form 28 April 1989)

Laboratory experiments and analysis of shallow water equations in a rotating fluid show that channel flow is governed by the ratio of the width of the channel to the Rossby radius of deformation $R=\sqrt{[g\Delta\rho H/\rho f^2]}$. Flows through narrow ocean openings exhibit blocking and clear evidence of hydraulic control. These imply that formulae can be derived for width, volume flux, and velocity scales of the currents. A new version of the constant potential vorticity problem is solved, and it is shown to predict volume flux within 22% of the zero potential vorticity results. Next a systematic method of predicting volume flux through ocean passages is described. Some examples are given from the Denmark Straits overflow and the flow of Antarctic Bottom Water into the western Atlantic Ocean. Two-layer flows and counter-flows with rotation in a narrow passage, the so-called lock exchange flow problem, duplicate flows at a number of important straits and openings to bays. A potential vorticity formulation is reviewed. The flows in the mouths of various bays such as Funka Bay in Hokkaido, Japan, Spencer Gulf in South Australia, and Chesapeake Bay in the United States has $R<$ width of the mouth, and the two currents are separated by a front. The width of the front and the density difference can be predicted with good results.

KEY WORDS: Rotating fluids, shallow water equations, channel flow.

1. INTRODUCTION

A simple model of the ocean, suggested by Stommel (1962) and studied by Rossby (1965), Beardsley and Festa (1972), and Speer and Whitehead (1988), consists of a rectangular box with differential heating on its top (Figure 1a). In such a fluid, sinking regions are found over a restricted area near the cold end (polar regions), the cold water then migrates equatorward along the bottom in a divergent flow which feeds vertical flow that rises through the thermocline. Thermal energy in that region has an advective/diffusive balance. Unfortunately, to a first approximation the ocean bottom at approximately 5000 m is not uniform. All deep ocean basins are separated by either mid-ocean ridges which typically are 2500–3500 m deep, hot spot traces of approximately the same depth, or combinations of the above with continental fragments which can be much shallower. This suggests a modified box model (Figure 1b) in which the bottom of the box is divided into deep basins with a substantial barrier extending upward from the bottom. The flow pattern differs substantially from the old model. In order to flow from the

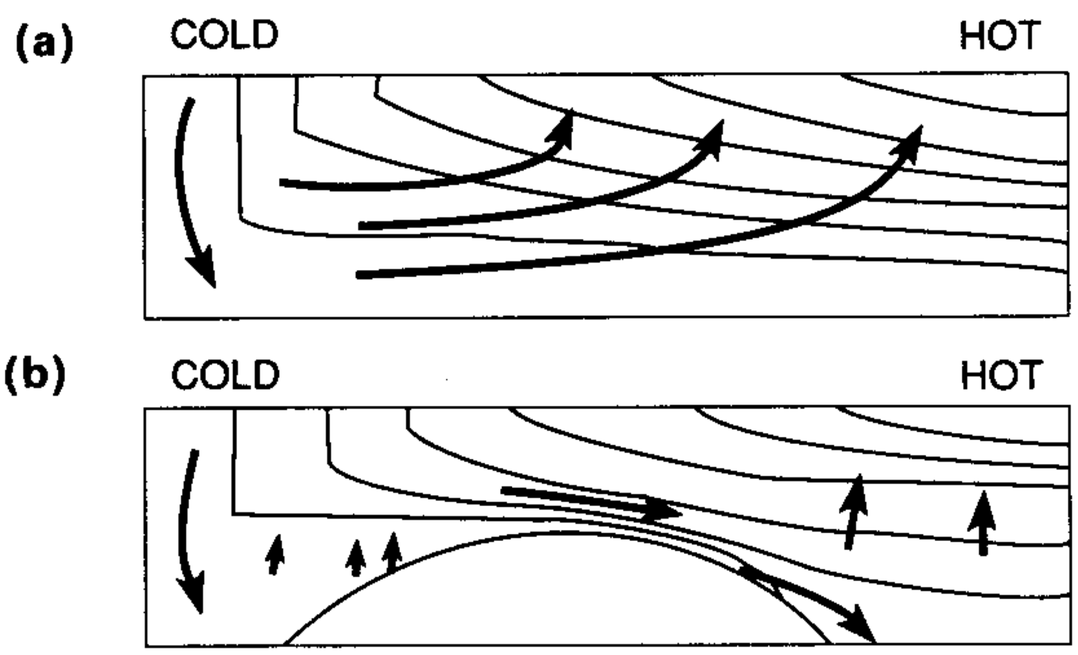

Figure 1 Two simple box models of the vertical circulation in an ocean. (**a**) In an ocean with no bottom topography, the sinking regioin is restricted to a small volume near the polar region. Cold water thus emplaced near the bottom then spreads to temperate latitudes and gradually rises, forming a thermocline. (**b**) With bottom topography, the cold water must first rise up over a sill, where it pours towards temperate latitudes as a concentrated current. This concentrated inertial current can be strongly influenced by earth's rotation.

basin with deep water formation to the next one, water must rise throughout the first basin and flow into the next basin at sill depth. The flow at the sill is localized, rapid, horizontal, and serves as a source of bottom water to the next basin. Thus the water flowing into the next basin is denser than water at sill depth in that basin.

Numerous ocean features suggest this concept. Figure 2 shows a north–south section (from GEOSECS), with interpretive arrows for current direction drawn in. In the North Atlantic, water formed in the Norwegian Sea fills the basin north of the Denmark Straits, and spills southward and down into the deep North Atlantic. In the South, water in the Argentine Basin flows over the Vema Passage on the Rio Grande Rise into the Brazil Basin. From this, warmer water flows over the Ceara Abyssal Plain into the North Atlantic. A plan view of the two density currents entering the North Atlantic is visible in Figure 3, which shows the two tongues of water colder than 1.7 °C (Potential Temperature) extending down into the North Atlantic. The northern one is fed by the Denmark Straits current and the southern one is fed by the current over the Ceara Abyssal Plain. It also shows a current going through the Romansch Fracture into the eastern Atlantic.

The purpose of the next part of this paper is to discuss and extend models of the dynamics near the crest of sills (Section 2) that act as passageways for these currents. A new formulation for constant potential vorticity will be shown, and compared to the zero potential vorticity formulation by Whitehead *et al.* (1974). Volume flux of the two results differs by only 22% or less, which implies that volume flux estimates are relatively insensitive to the potential vorticity of the upstream water. A methodology to test these predictions against oceanic data will then be advanced and a few test examples for oceanic flows will be discussed (Section 3).

Next, balances suggested by the lock-exchange or two-way flow will be analyzed. In Section 4, a solution using the assumption of zero potential vorticity will be reviewed. A methodology to test these predictions against oceanic data will

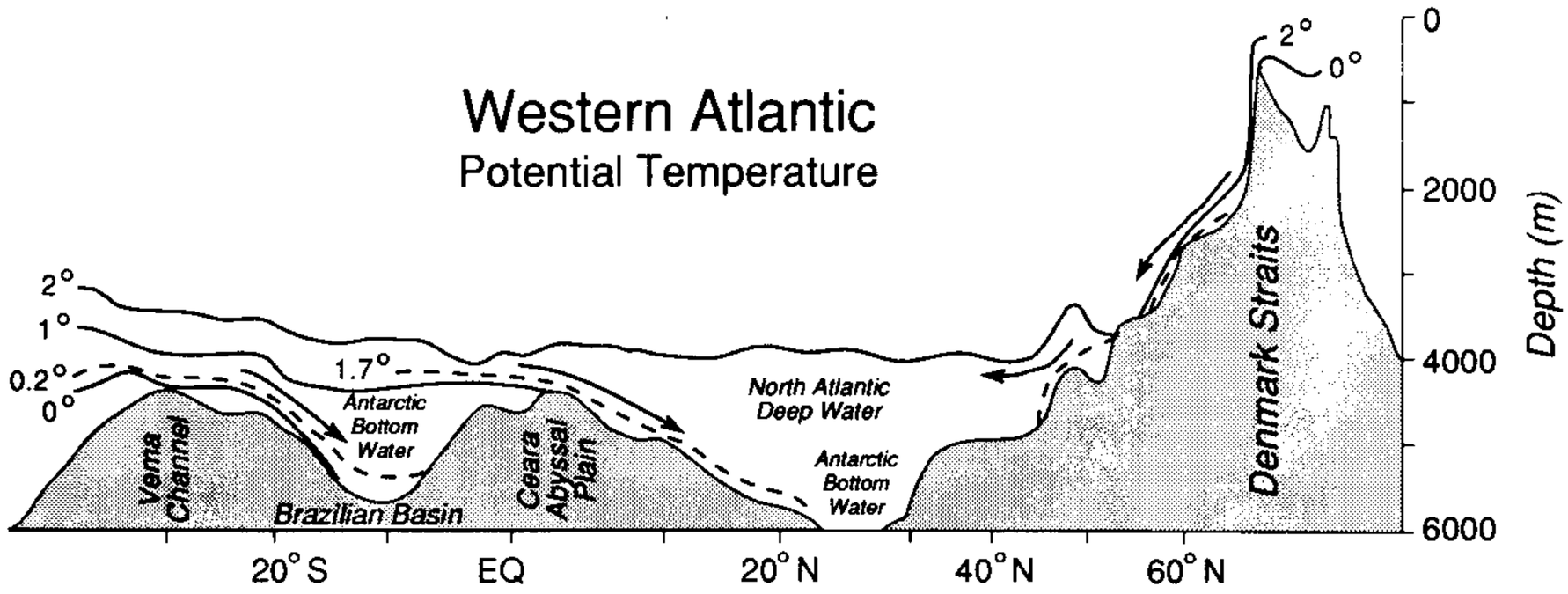

Figure 2 Elevation view of selected isotherms in the western North Atlantic, with three sill flows shown as arrows. The bathymetry between 20 and 40° South has been redrawn to show more accurately the depth of the deepest portion of the ocean.

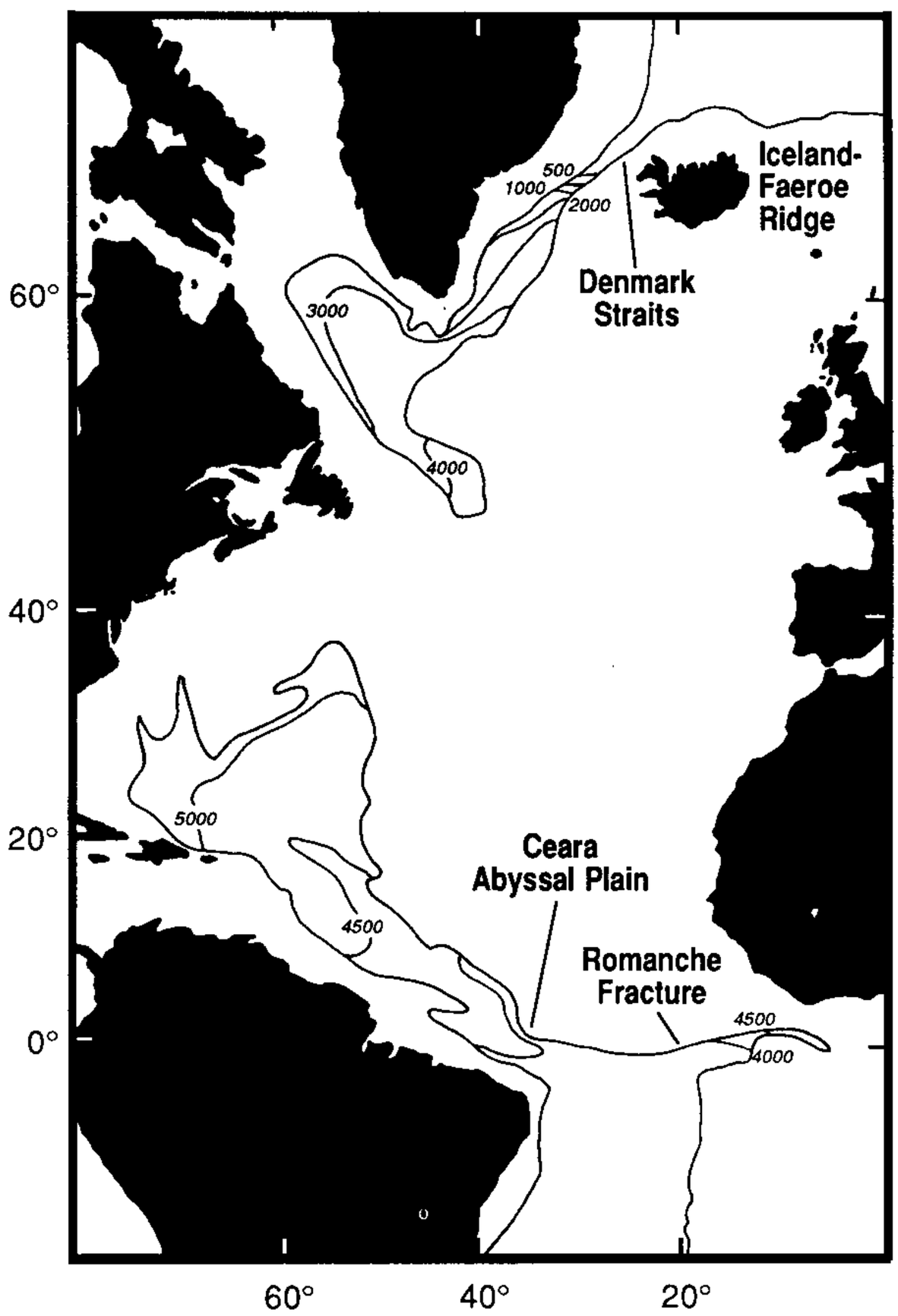

Figure 3 Plan view of the depth of the 1.7° potential temperature surface in the western North Atlantic. The transition from a level surface to a sloping surface reveals two sill flows.

be described. The results will be tested against the flows in the mouths of two bays in Section 5.

2. CONTROL OF ONE LAYER

Whitehead *et al.* (1974) and Gill (1977) present several general solutions to the problem of the flux of a rotating fluid flowing from an upstream basin through a rectangular channel. The flow rate is controlled in the sense that if the geometry of the channel were changed, the volume flux through the channel would be changed, so that the jets and currents out of the upstream basin must change. Whitehead *et al.*, present the case of the upstream basin as very deep compared to the sill depth, which led to the assumption of zero potential vorticity. The solutions were explicit algebraic functions for the predicted quantities such as width of the current, volume flux, parameter for transition from small to fast rotation, etc. Gill extended the solutions to the case of smaller upstream depth, which is an assumption of constant potential vorticity. The results were relatively complicated mathematically. It was necessary to postulate one or two coastal currents in the upstream basin, and the solutions were the roots of eighth order polynomials whose values were obtained numerically for only specific values of the governing parameters. Thus it was not possible to directly compare the constant and the zero potential vorticity predictions for volume flux through the opening as a function of the external parameters. Shen (1981) showed experimentally that flux was relatively insensitive to upstream vorticity. Thus it seems useful to determine exactly how much the zero and constant potential vorticity fluxes differ. Pratt and Armi (1987) inspected numerous flows with non-constant potential vorticity. Numerous complicating aspects arise, but effect on the volume transport is unclear.

Here we present a new solution for a constant potential vorticity flow. The prediction for volume flux can be directly compared with the zero potential vorticity case of Whitehead *et al.*, in order to determine how sensitive volume flux is to the upstream potential vorticity.

Consider the following situation with geometry shown in Figure 4: A flat plain in a rotating system with gravity downward is bounded laterally by two walls that form a channel of width $L(y)$, such that $L(y)$ is a minimum L at $y=0$ and $L(y)$ tends to infinity at $y\to-\infty$. A sliding gate blocks at $y=0$ so that there is fluid of density $\rho+\Delta\rho$ and depth $=H$ at $y<0$ and no fluid at $y>0$. Let the left-hand wall (looking toward $+y$) be straight and located at $x=0$.

When the gate is removed, Gill (1977) conjectured that a Kelvin wave propagates along the wall, readjusting the interface height $h(x)$ and setting up a constant potential vorticity density current flowing with velocity $v(x)$. The shallow water equations for the steady current are:

$$\mathbf{u}\cdot\nabla\mathbf{u}+f\hat{\mathbf{k}}\times\mathbf{u}=g'\nabla h, \tag{2.1}$$

and continuity is

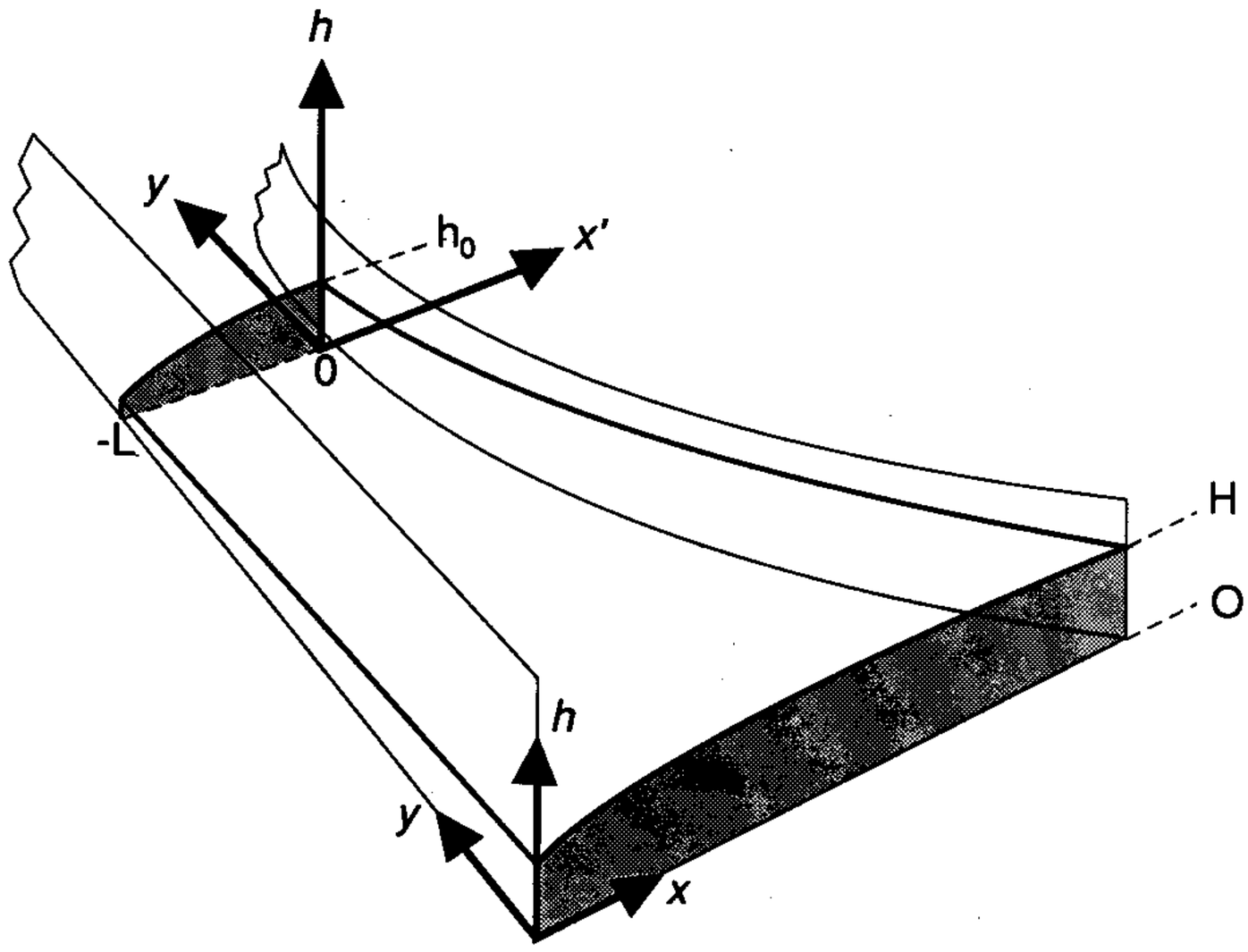

Figure 4 Sketch of the geometry of the constant potential vorticity problem. A reduced gravity current comes from $y=-\infty$ where the channel is very (infinitely) wide along a flat bottom to a point where the channel is width L.

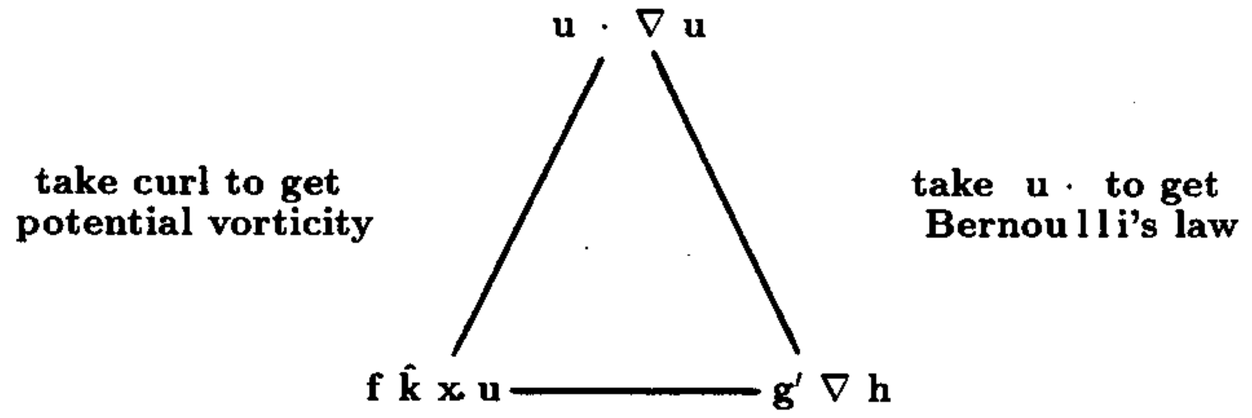

Figure 5 Triangle diagram used to illustrate the three different combinations of equations that result from the general equations.

$$\nabla \cdot \mathbf{u}h = 0. \tag{2.2}$$

It is usual to work with conserved quantities such as potential vorticity

$$\frac{1}{h}\left(\frac{\partial v}{\partial x} - \frac{\partial u}{\partial y} + f\right) = F(\psi) \tag{2.3}$$

which is found by taking the curl of (2.1) (thereby eliminating the right-hand term) and using (2.2). Here $F(\psi)$ can be regarded as upstream potential vorticity which is a function of streamfunction ψ defined as

$$\nabla \times \psi \hat{\mathbf{k}} = h\mathbf{u}. \tag{2.4}$$

If one integrates along streamlines, the middle term (2.1) is eliminated since it has zero component in the flow direction. Bernoulli's law holds

$$\frac{v^2}{2} + g'h = G(\psi). \tag{2.5}$$

It is well known that $\partial G/\partial\psi = F$, and this is an important condition to be used in specifying the flow in the upstream basin. One can show that for a channel flow, (2.3) and (2.4) imply that rectilinear flow is geostrophic. This balance can be recovered by seeking the component perpendicular to a uniform flow in (2.1) in which case the first term of (2.1) is eliminated.

For the case of a straight channel, the geostrophic balance is

$$fv = g' \frac{\partial h}{\partial x}. \tag{2.6}$$

Only when $\partial G/\partial\psi = F$ will (2.6), (2.5) and (2.3) be compatible.

It is often helpful to visualize the assorted manipulations described above in terms of a triangle diagram shown in Figure 5. This is particularly useful when one initiates new studies, for instance, flows with new geometries.

Neglecting y derivatives (and thus assuming that the channel geometry is slowly varying), the vorticity equation is

$$\frac{1}{h}\left(\frac{\partial v}{\partial x} + f\right) = \frac{f}{H}, \tag{2.7}$$

which is combined with (2.6) to give

$$\frac{\partial^2 h}{\partial y^2} - \frac{f^2}{g'H} h = -\frac{f^2}{g'}, \tag{2.8}$$

with solution

$$h = H - A\, e^{-x/x_0} - B\, e^{x/x_0}, \tag{2.9}$$

where

$$x_0 = \sqrt{\frac{g'H}{f^2}}. \tag{2.10}$$

Far upstream ($y \to -\infty$), where the channel is becoming infinitely wide, only decaying solutions can be permitted in the plus x direction, so $B = 0$ and (2.9) reads

$$h_u = H - \eta e^{-x/x_0}, \tag{2.11}$$

where η is undetermined. It is well known (Gill, 1977) that the Bernoulli function is proportional to the streamfunction for this problem and is, in general, unknown. However, its value is $g'H$ as $x \to \infty$, because velocity is zero there. Let us now investigate conditions at the opening of width L. Since Bernoulli function is conserved along streamlines, the upstream value of the Bernoulli function on the right-hand wall $g'H$ will be the value of the Bernoulli function on the right-hand wall at *any* location.

At the contraction itself, it is convenient to adopt a coordinate system with origin x' on the right-hand wall because that point has the known Bernoulli function. We represent the solution as

$$h = (h_0 + A + B) - A e^{-x'/x_0} - B^{x'/x_0}, \tag{2.12}$$

where h_0 is fluid height on the right-hand wall. Note that, since (2.9) holds everywhere

$$h_0 + A + B = H. \tag{2.13}$$

The velocity v_0 on the right-hand wall is found using the geostrophic balance at $x = 0$ in (2.12)

$$v_0 = \frac{g'}{f}\frac{\partial h}{\partial x} = \frac{g'}{f x_0}(A - B). \tag{2.14}$$

Bernoulli's law at $x = 0$ gives

$$\tfrac{1}{2}v_0^2 + g'h_0 = g'H, \tag{2.15}$$

so

$$v_0 = \sqrt{[2g'(H - h_0)]}, \tag{2.16}$$

using (2.10) and (2.14)

$$A - B = \sqrt{[2H(H - h_0)]}. \tag{2.17}$$

Using (2.13) this gives

$$A = \tfrac{1}{2}\{H - h_0 + \sqrt{[2H(H - h_0)]}\}, \tag{2.18}$$

and

$$B = \tfrac{1}{2}\{H - h_0 - \sqrt{[2H(H - h_0)]}\}, \tag{2.19}$$

so

$$h = H - \tfrac{1}{2}[H - h_0 + \sqrt{\{2H(H - h_0)\}}]\, e^{-x/x_0}$$

$$-\tfrac{1}{2}[H-h_0-\sqrt{\{2H(H-h_0)\}}]\,e^{x/x_0}, \tag{2.20}$$

and

$$v=\frac{1}{2}\sqrt{\frac{g'}{H}}\{[H-h_0+\sqrt{\{2H(H-h_0)\}}]\,e^{-x/x_0}$$

$$-[H-h_0-\sqrt{\{2H(H-h_0)\}}]\,e^{x/x_0}\}. \tag{2.21}$$

Volume flux is

$$Q=\frac{g'}{2f}[h(0)^2-h(-L)^2]$$

$$=\frac{g'}{2f}\{h_0^2-[H-\tfrac{1}{2}[H-h_0+\sqrt{\{2H(H-h_0)\}}]\,e^{-L/x_0}$$

$$-\tfrac{1}{2}[H-h_0-\sqrt{\{2H(H-h_0)\}}]\,e^{L/x_0}]^2\}. \tag{2.22}$$

Let $h_0/H=\gamma$

$$Q=\frac{g'}{2f}H^2\{\gamma^2-[1-\tfrac{1}{2}[1-\gamma+\sqrt{\{2(1-\gamma)\}}]\,e^{-x/x_0}$$

$$-\tfrac{1}{2}[1-\gamma-\sqrt{\{2(1-\gamma)\}}]\,e^{x/x_0}]^2\}. \tag{2.23}$$

This equation has been solved by direct calculation and results are shown in Figures 6 and 7. Figure 6 shows contours of normalized volume flux $2Qf/g'H^2$ (which we will call flux for simplicity) as a function of the free parameter h_0/H and the normalized width of the channel L/x_0. For a given width, there is a maximum flux denoted by the point where the contour of constant flux becomes vertical. The value of h_0/H at this point of maximum flux is shown by a dashed line and lies between 2/3 (the critical value at zero rotation) and 1. We assert that, at the point of minimum channel width, critically controlled flow will adopt this value of h_0/H. This assertion is based upon numerous arguments, two of which will be given here.

One argument is that the fastest waves will be frozen in the flowing fluid at the point of contraction, or equivalently that some suitably averaged cross-stream velocity at the contraction point will be at the speed of the fastest wave which, in this case, is the longest wave. Shorter waves will propagate more slowly and will consequently be swept downstream. Therefore, no information can propagate from the region downstream of the maximum contraction to the region upstream of the contraction. Gill (1977) showed that maximizing flux results in a frozen wave at the contraction by the following argument: Since the long waves are simply a local variation of h_0/H at fixed L/x_0, only if h_0/H is at the value which gives maximum flux will small variations (*i.e.*, waves) in h_0/H have no along-stream changes in flux. Conversely, if h_0/H is at a value that does not give maximum flux, so that

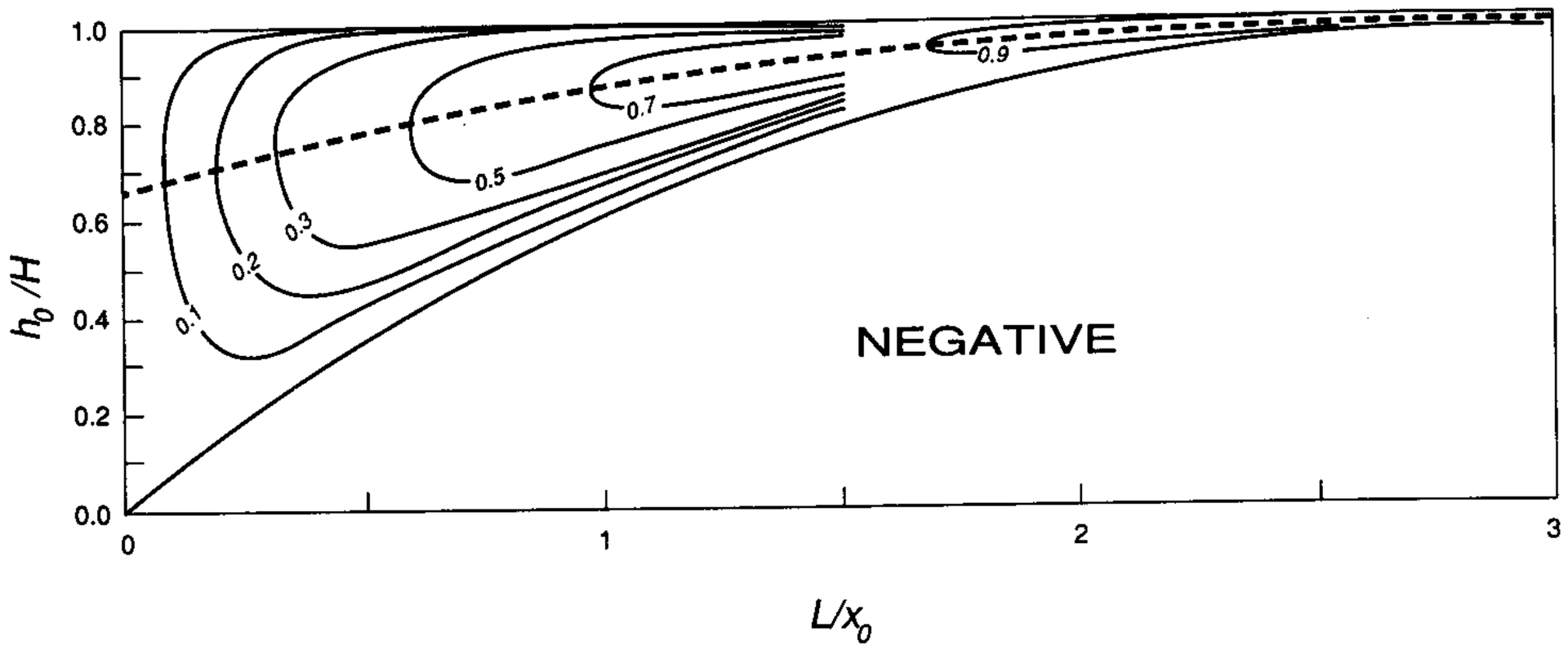

Figure 6 Contours of flux as a function of the normalized depth of the fluid on the right-hand wall and normalized channel width.

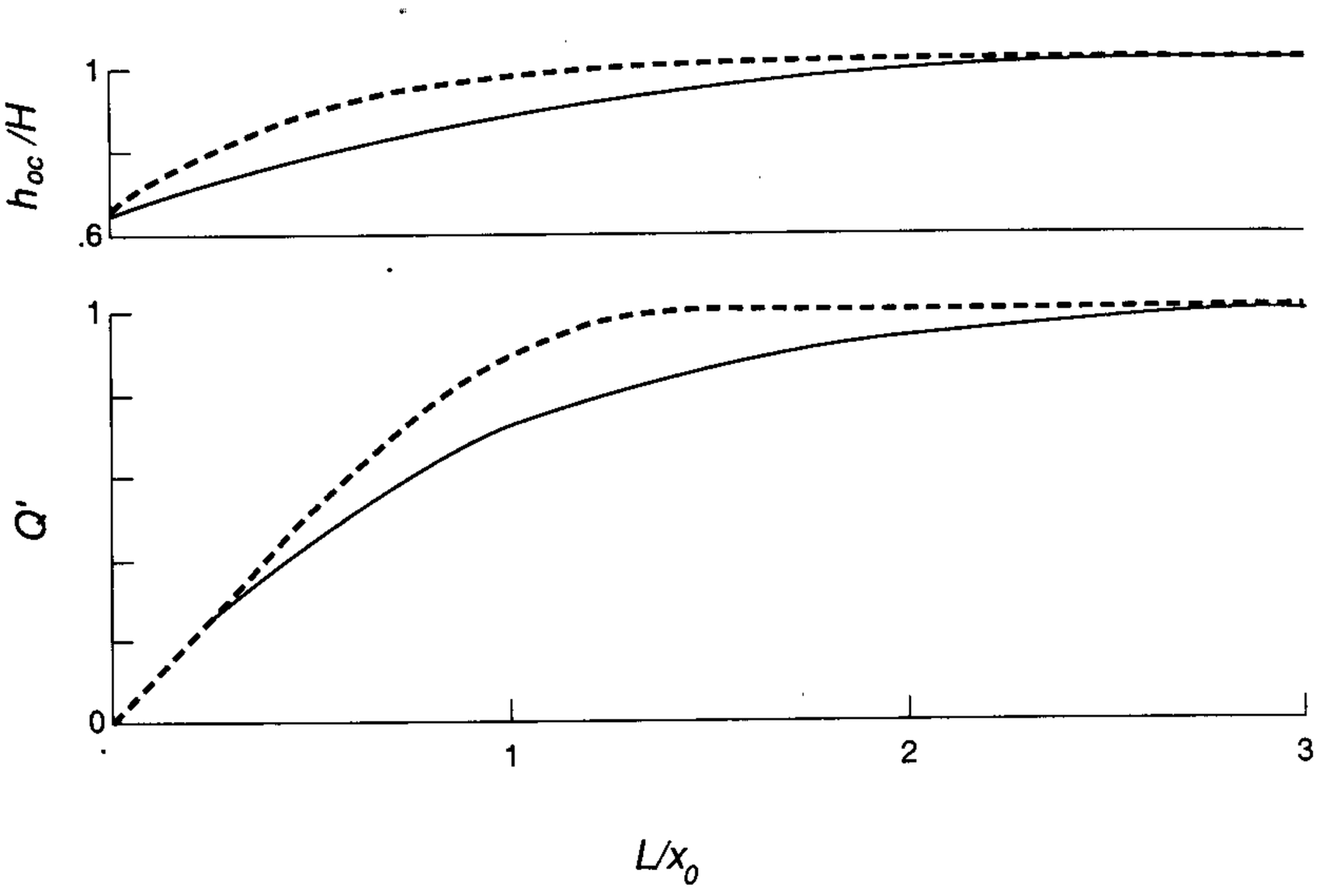

Figure 7 Flux and critical depth as a function of channel width for constant potential vorticity (solid) and zero potential vorticity (dashed).

local variations in h_0/H produce volume flux changes along-stream, there must be a time-dependent term in the cross-stream integrated continuity equation which will lead to a propagating wave solution.

This figure also illustrates a second, and in some ways, more convincing argument: If h_0/H lies on the dashed line, the current *must* decrease if L/x_0 is further decreased. One can see immediately why this is true. To the left of any point on the dashed line, the flux is always smaller. In contrast, if h_0/H does not lie on the dashed line, a decrease in L/x_0 can be accompanied by no change in flux if h_0/H is appropriately adjusted. Thus the maximum flux which is located along

the dashed line is associated with an unmistakable control by the width L/x_0, whose decrease *must result* in a smaller flux.

The values of critical flux and h_0/H as a function of L/x_0 are compared to the zero potential vorticity solution of Whitehead *et al.* (1974) in Figure 7. In their solutions, flux $=1$ if $L/x_0 > \sqrt{2}$, and flux $= 2(2/3)^{3/2}(L/x_0)(1-L^2/8x_0^2)^{3/2}$ otherwise. The constant slope of both the constant and the zero potential vorticity flux relations as L/x_0 goes to zero implies that flux is proportional to L. The slope for both cases becomes the same and is equal to the classical value for two-dimensional flow in non-rotating hydraulics—that volume flux per unit width is equal to $(2H/3)^{3/2}(g')^{1/2}$. This result is given in Whitehead *et al.*, for the zero potential vorticity flow and is found here by taking Eq. (2.23) in the limit L/x_0 small as follows: Approximately $e^{\pm L/x_0} = 1 \pm L/x_0$ so that

$$Q = \frac{g'H^2}{2f}\left\{\gamma^2 - \left[1 - \tfrac{1}{2}[(1-\gamma+\sqrt{\{2(1-\gamma)\}}]\left(1-\frac{L}{x_0}\right)\right.\right.$$

$$\left.\left. - \tfrac{1}{2}[1-\gamma-\sqrt{\{2(1-\gamma)\}}]\left(1+\frac{L}{x_0}\right)\right]^2\right\}, \tag{2.24}$$

$$= \frac{g'H^2}{2f}\left[\frac{2\gamma L}{x_0}\sqrt{\{2(1-\gamma)\}}\right]. \tag{2.25}$$

In dimensional form this is

$$Q = h_0 L\sqrt{\{2g'(H-h_0\}}, \tag{2.26}$$

which is the prediction from classical hydraulics with non-rotating fluid. Critical $h_{0_c} = \frac{2}{3}H$ and volume flux is

$$Q = \left(\frac{2H}{3}\right)^{3/2} L\sqrt{g'}. \tag{2.27}$$

Both zero and constant potential vorticity curves for flux also approach each other as L/x_0 gets very large, as do the curves for h_0/H. This is simply due to the fact that in this limit, flux is controlled by the geostrophic relation where the depth remains at the upstream depth on one side of the channel and depth goes to zero on the other side. Greatest disagreement between the two cases occurs at intermediate values of L/x_0. Even there, volume flux predicted for the two very different potential vorticities varies by only 22%. This indicates that the values of the potential vorticity of the upstream fluid may have only a small effect on volume flux.

There are no empirical constraints needed in the calculation. The flux is independent of vertical or horizontal coefficients of turbulent diffusivity, conduc-

tivity or viscosity, but are valid only when friction and thermal conduction are negligible. Such a situation exists when the residence time of a fluid parcel in the flowing water is less than spin-down time of the fluid parcel $d/\sqrt{(vf)}$, where d is the depth of the fluid. Since velocity scales as $\sqrt{g'd}$, residence time of a parcel is $w/\sqrt{(g'd)}$, where w is the length of the channel thus for $w/\sqrt{(g'd)} < d/\sqrt{(vf)}$ we require

$$\frac{w}{d} < \sqrt{\frac{g'd}{vf}}. \tag{2.28}$$

This is easily satisfied in the laboratory. Using $g' = 0.1\,\mathrm{m/s^2}$, $d = 0.1\,\mathrm{m}$, $v = 10^{-6}\,\mathrm{m^2/s}$ and $f = 1\,\mathrm{s^{-1}}$, we require $w < 10\,\mathrm{m}$. The application to the ocean examples will be commented on at the end of the next section.

3. A METHODOLOGY OF TESTING AGAINST OCEAN DATA

Although the original formulae in Whitehead *et al.* (1974) were tested against oceanic numbers, little use has been made of these formulae by ocean scientists since that time. In fact, a number of ocean studies have been published which have not discussed predictions of his model in comparison with their data at all. In hopes of clarifying the way in which this model could be used, a methodology is developed here which will be applied to four examples.

Now that we have seen that volume flux is relatively insensitive to upstream vorticity, we will predict volume flux using the formulae from Whitehead *et al.* (1974)

$$Q = \frac{g' h_u^2}{2f} \quad \text{for} \quad \frac{(2g'h_u)^{1/2}}{f} < b, \tag{3.1}$$

and

$$Q = \left(\frac{2}{3}\right)^{3/2} b (g')^{1/2} \left[h_u - \frac{f^2 b^2}{8g'} \right]^{3/2} \quad \text{otherwise.} \tag{3.2}$$

These were shown to be within 22% of the constant potential vorticity example developed in the preceding section, but are simpler algebraically. The examples to be selected have oceanographic estimates of volume flux which can be compared to our predictions. Application of the theory to the ocean relies on the adoption of estimated numbers for: (1) density difference between the flowing and overlying fluid $\Delta\rho/\rho$, (2) upstream height over the sill $h_u = \sqrt{(2g'h_u)}/f$, (3) channel width b, and (4) Coriolis parameter. Since the theory neglects friction, we can regard the predictions as giving an upper bound. Thus in all cases, estimates of the parameters will be taken that lead to the greatest predicted volume flux. (1) To estimate $\Delta\rho/\rho$, we will select two density profiles, one on each side of the sill. The profiles should extend 200 m below the sill depth on each side so that spurious

effects from the bottom are avoided. Values of density should be adiabatically corrected for pressure to the closest 1000 m level. The value of $\Delta\rho/\rho$ will be picked after determining sill depth. (2) To determine upstream height, the sill depth z_s should be determined from modern bathymetry charts. The two density-versus-height curves should be drawn on a ρ-versus-depth and a horizontal line drawn at the sill depth. The density difference should be picked as the greatest density difference between this level and higher up. The depth z_d at which the two curves begin to differ, should be located and h_u assigned as $z_d - z_s$. (3) The value of b should be determined as the width of the sill at z_d. (4) Coriolis parameter will be taken as $f = 1.44 \times 10^{-4} \sin\theta$, where θ is latitude.

This method will now be applied to four oceanic sills. The first two are the Denmark Strait that lies between Iceland and Greenland and the ridge between Iceland and the Faeroe Islands. These two dam up the deep Norwegian Sea water and prevent its flux southward at depths greater than approximately 600 m. The third is the Ceara Abyssal Plain near the Equator in the Western Atlantic. This dams up northward flowing dense water of Antarctic origin (called loosely Antarctic Bottom Water) at depths greater than roughly 4300 m. The fourth is the ridge between the Rio Grande Rise and the Sao Paolo Plateau near 30° south. This ridge contains a depression called the Vema Channel and also dams up the Antarctic Bottom Water at depths greater than roughly 4600 m.

This methodology has the virtue that only two sources of ocean facts are needed. The first is the best possible map with which to locate and outline the contour of the sills. The second is a source of precise data on the density distribution of oceanic water on both sides of the sills. Two maps were used: For the Denmark Strait and the Iceland–Faeroe sill the bathymetric chart of the Norwegian Sea and adjacent areas by Eggvin *et al.* (1963) was employed. (Our version had a factor of 10 error on the horizontal scale that was presumably a typographical error. Thus we ignored the scale and used latitude and longitude lines to determine lateral lengths.) For the Ceara Abyssal Plain and the Vema Channel, the map "Bathymetry of the Continental Margin of Brazil" by Moody *et al.* (1979) was used.

In order to use a consistent data set for vertical density distribution, we wished to use only GEOSECS data. For both maps we traced the most important bathymetric contours and also located the stations from GEOSECS as shown in Figures 8 and 9. From the apparent location of the sills, shown as dashed lines, we produced the cross-sections of the four sills that are shown in Figures 10–13. The data from each sill was determined from the above figures. Each is now to be discussed in turn, and the numbers summarized in Table 1.

To determine density in the vicinity of the Denmark Strait overflow, station 11 downstream of the sill and station 15 upstream of the sill from GEOSECS were used. These are shown along with the local bathymetry in Figure 8. As shown in Figure 10, the top of the density difference between upstream and downstream z_d is at 70 m depth—very close to the upper surface. In fact, the upper water is extremely variable both seasonally and spatially due to seasonal and coastal effects. The sill depth z_s, is 650 m, the same number used by Whitehead *et al.* (1974). This gives $h_u = 580$ m, and a density difference of 3×10^{-4}. The Rossby

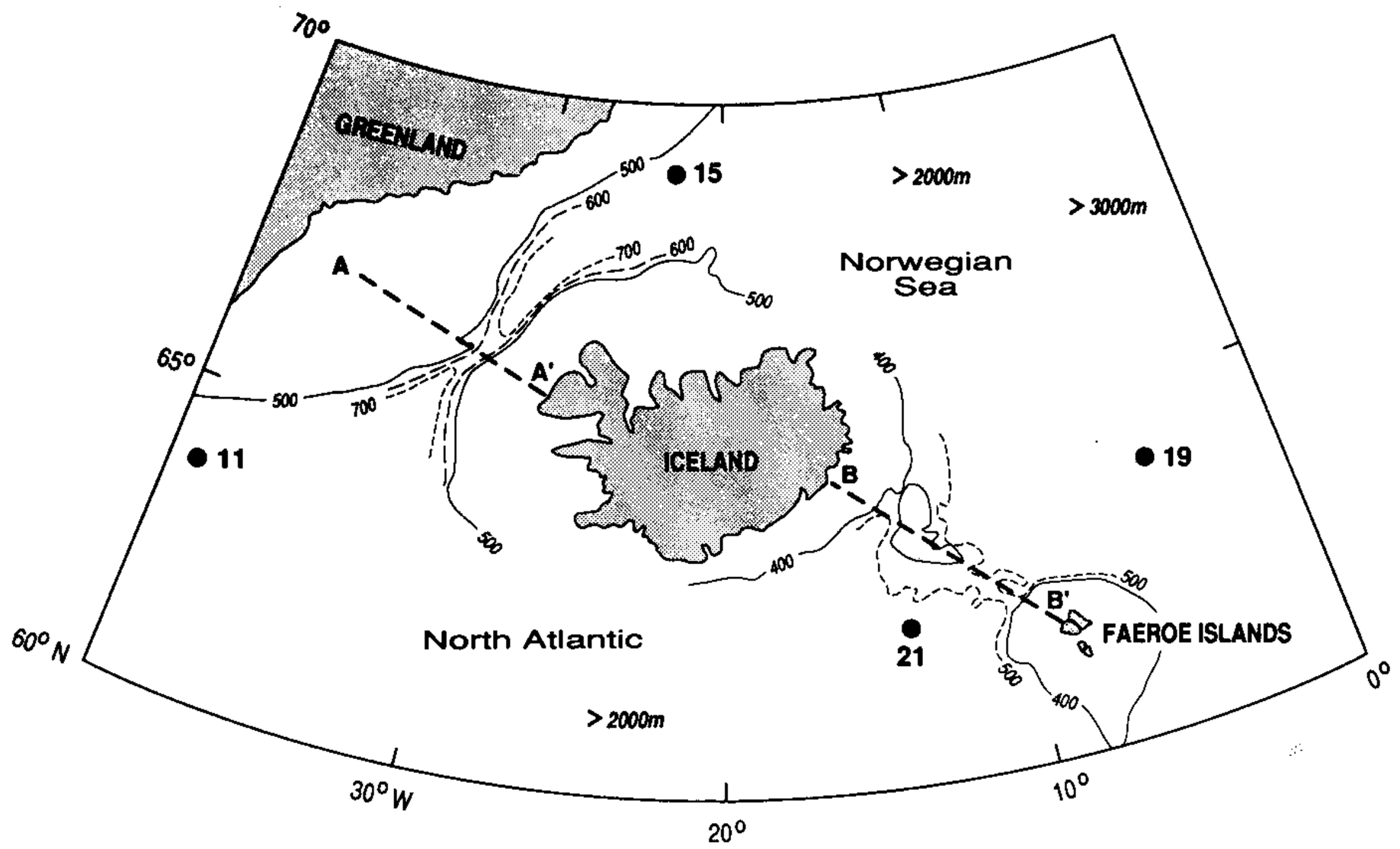

Figure 8 Map showing the two sills between Greenland and the Faeroe Islands along with selected bathymetric contours (in metres) and the locations of GEOSECS stations used for data.

radius $x_b = 14$ km which is considerably less than $b = 350$ km so that Eq. (3.1) (the high rotation rate formula), is used to calculate $Q = 3.9$ Sv (1 Sv (Sverdrup) $= 10^6$ m^3/s is a common oceanic unit of volume flux, and will be used throughout).

There have been numerous attempts to measure the flux of this water. Dietrich (1957) used dynamic computations to estimate that 5.6×10^6 Sv flows southward. Worthington (1969) attempted to measure the current with a moored current meter array but most of the moorings were not retrieved. He suggests a transport of "probably 4 Sv" but noted that the data were not sufficient and also noted the possibility of strong bursts. Ross (1976) describes current meter measurements taken in 1973 for 36 days. The transport was observed mostly as bursts with a peak of 7 Sv. The mean was given as 2.5 Sv. These current measurements are less than our estimates (which should be regarded as an upper bound). The earlier geostrophic estimates are greater than our estimate. It is hard to imagine why this is so since geostrophy is used in the rotating hydraulics. Possibly the dynamic sections were taken downstream where the current has been swollen by turbulent entrainment.

The second sill is the Iceland–Faeroes overflow. The density profiles selected were stations 19 (upstream) and 21 (downstream). These are shown along with the local bathymetry in Figure 8. Figure 11 shows the profile of the sill region with the two density distributions from which a value of $h_u = 400$ m and a density difference of 5.8×10^{-4} was taken. Using the local Coriolis parameter, the Rossby radius is $x_b = 17$ km whereas the sill width is $b = 400$ km. Thus Eq. (3.1) gives $Q = 3.6$ Sv.

Steele *et al.* (1962) used Swallow (neutrally buoyant) floats in conjunction with

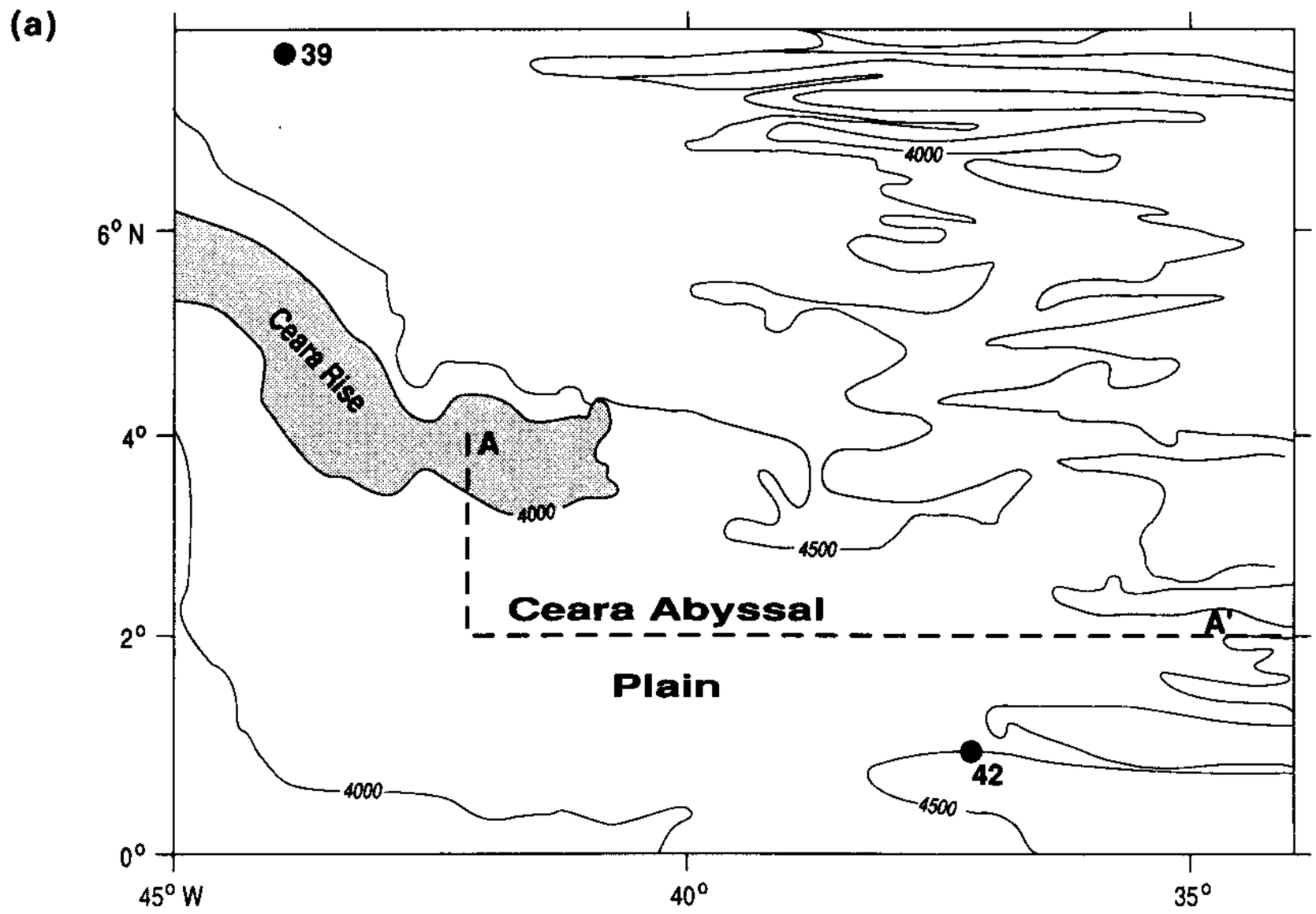

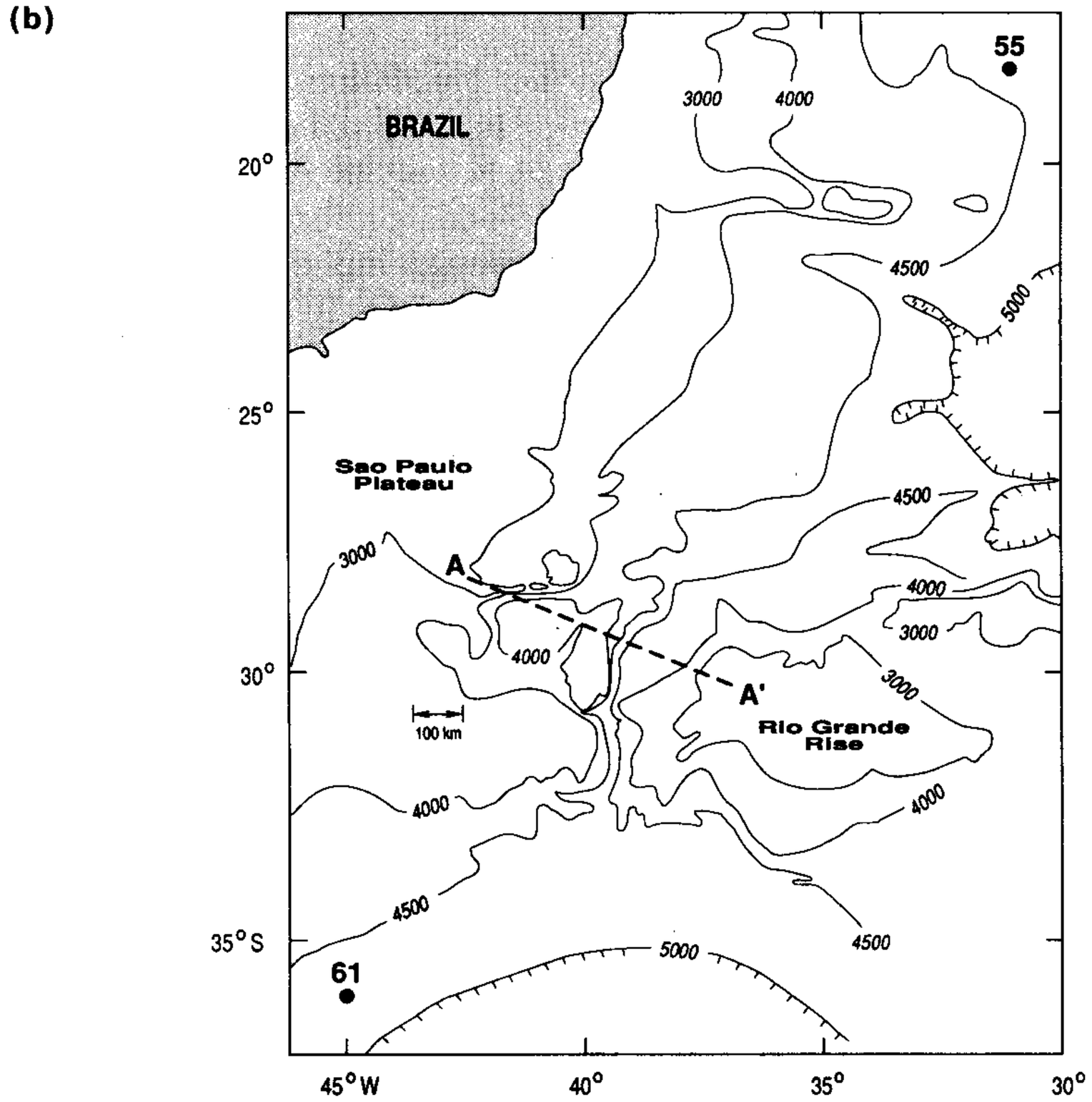

Figure 9 Maps showing selected bathymetric contours (in metres) and the locations of GEOSECS stations at (**a**) roughly 4° North and (**b**) roughly 30° South in the deep ocean east of Brazil.

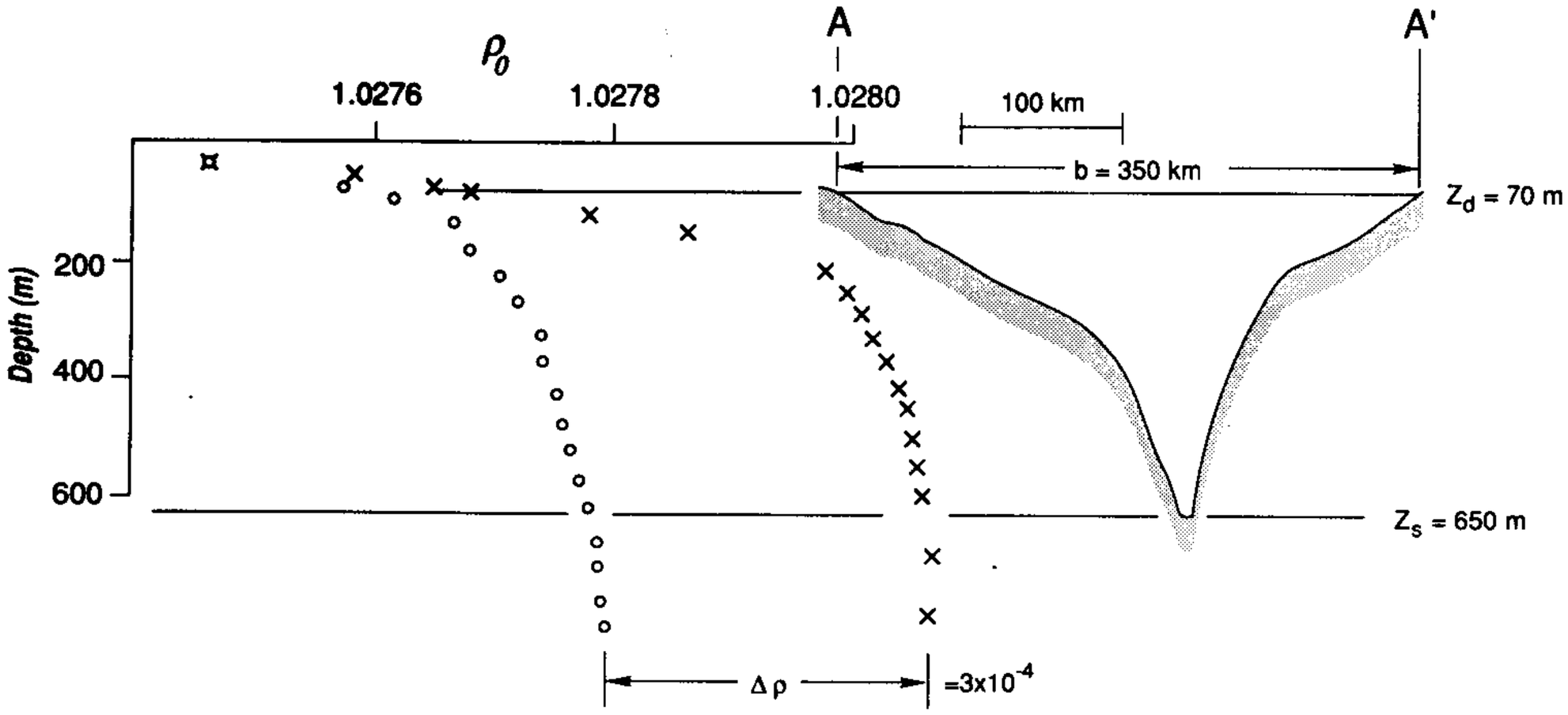

Figure 10 Elevation view of the Denmark Strait at the section shown by dashed line in Figure 8 along with density from the two GEOSECS casts. ×: upstream; ○: downstream.

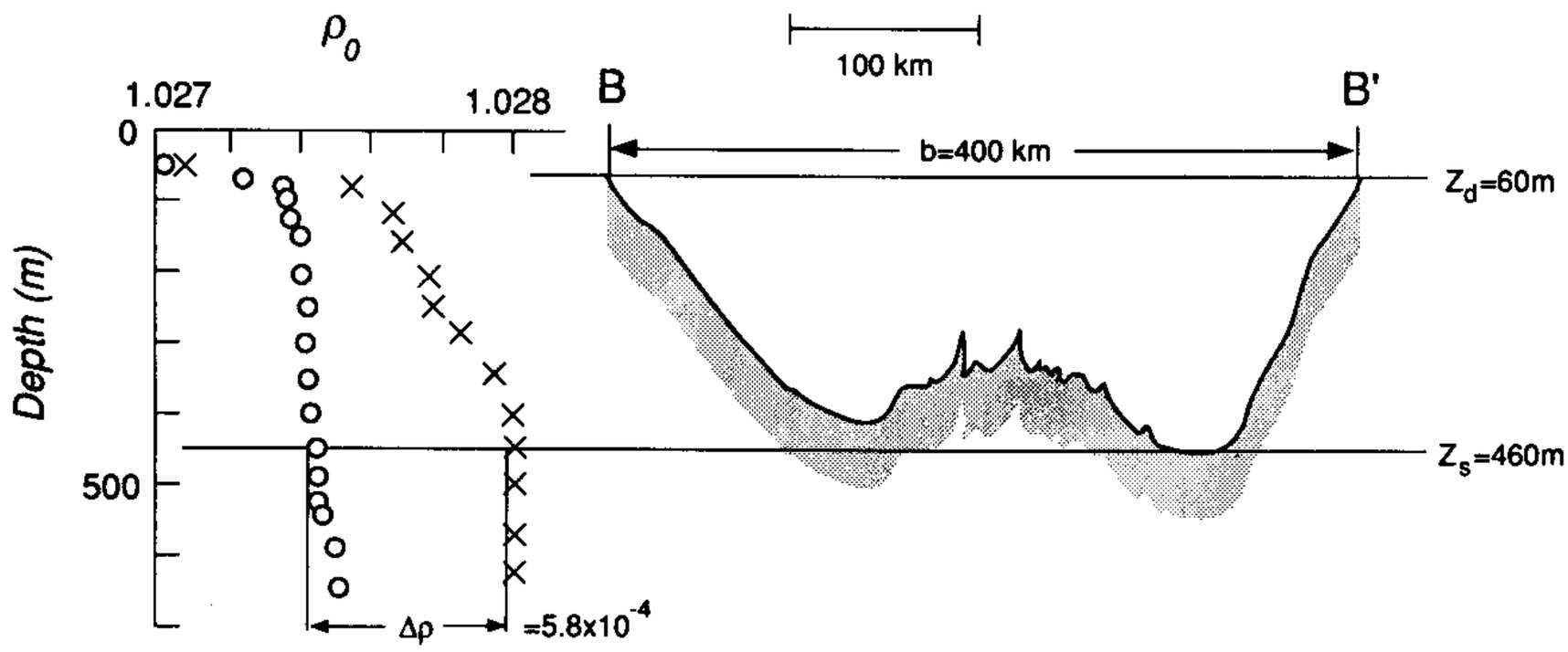

Figure 11 Elevation view of Iceland–Faeroe sill at the section shown by a dashed line in Figure 8 along with density from the two GEOSECS casts. ×: upstream; ○: downstream.

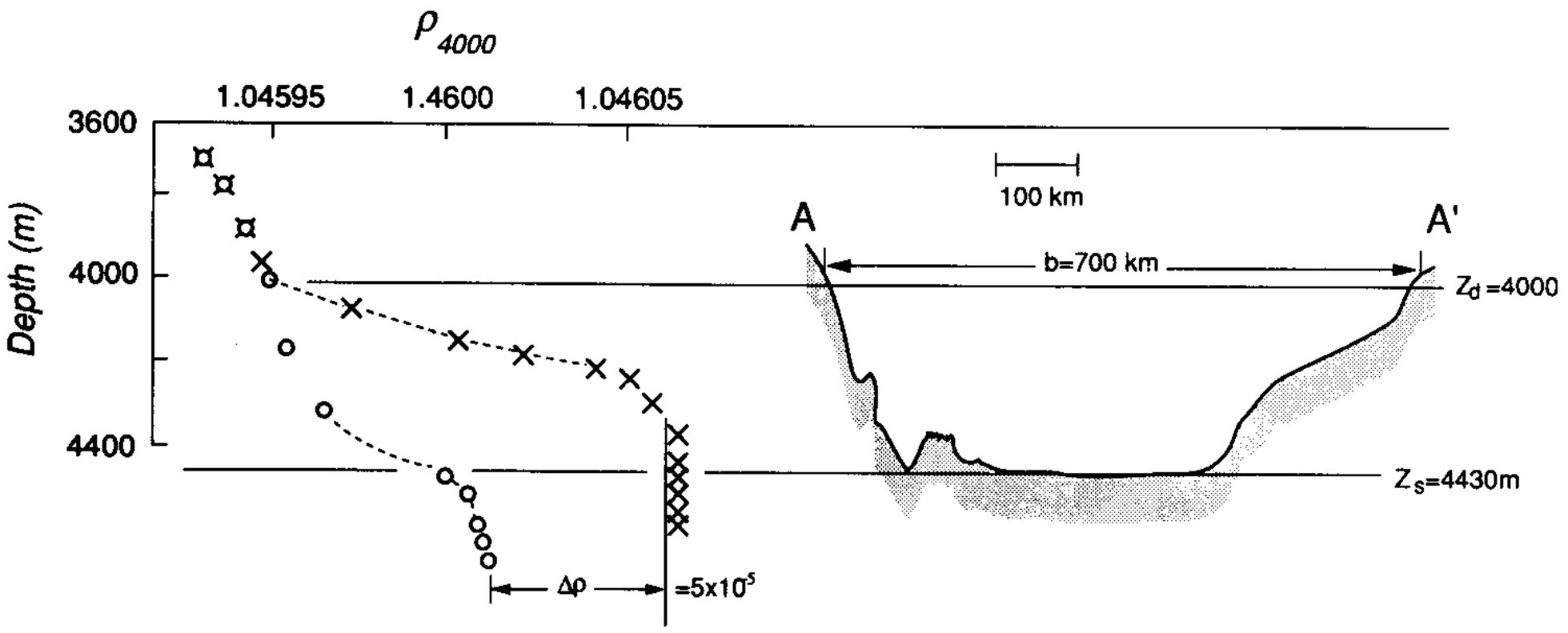

Figure 12 Ceara Abyssal Plain sill at the section shown by a dashed line in Figure 9(a) along with density from two GEOSECS casts. ×: upstream; ○: downstream.

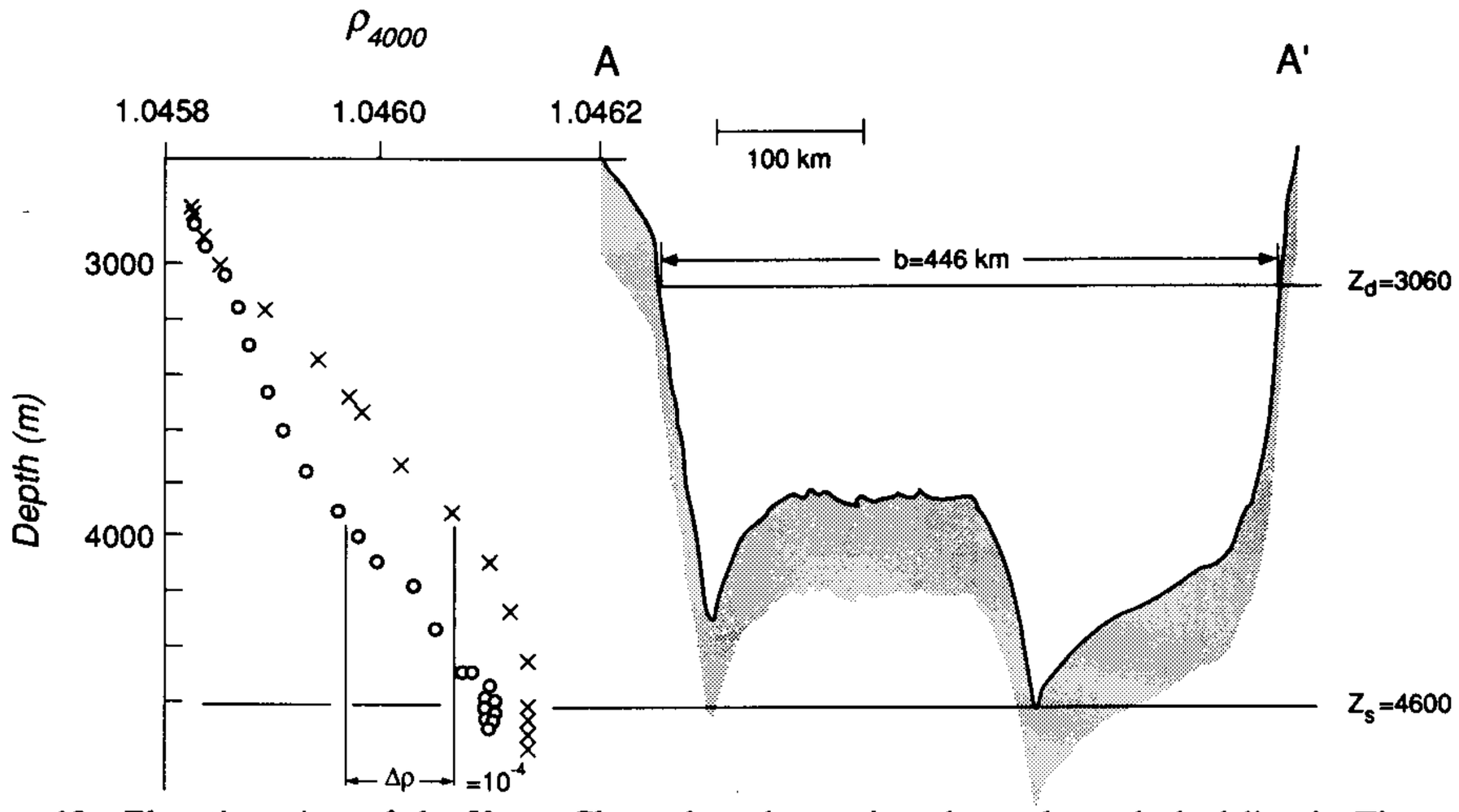

Figure 13 Elevation view of the Vema Channel at the section shown by a dashed line in Figure 9(b) along with density from the two GEOSECS casts. ×: upstream; ○: downstream.

dynamic calculations to estimate a transport of water on the continental slope south of Iceland as 5.4 Sv of which they estimate 1.4 Sv was flux of water from the Norwegian Sea (which by continuity must have flowed over the Iceland–Faeroe ridge) and 4.0 Sv was entrained Atlantic Water. Our estimate is considerably greater than this. Direct measurements with current meters have not been made to date.

The third sill is at the northern terminus of the Ceara Abyssal Plain. Bathymetry is shown in Figure 9a along with locations of the section and stations. The density profiles selected were stations 39 (downstream) and 42 (upstream) of GEOSECS. These are shown in Figure 12 along with values of $\Delta\rho$ and z_d. The sill configuration is taken from Figure 6a. Depth of the water, h_u is 430 m. This gives a value of Rossby radius $x_b = 66$ km which is much less than $b = 700$ km. Thus Eq. (3.1) gives $Q = 4.6$ Sv.

Whitehead and Worthington (1982) measured a flux through the gap at 4 °N between 1.1 and 2.1 Sv which is considerably less. Part of the disagreement may be due to friction, for the isotherms exhibit a clear slope between station 42 (at the equator) and stations farther north where the bottom begins to deepen. However, an analysis of this is beyond the scope of this paper.

The last sill, called the Vema channel, lies between the Rio Grande Rise and the Sao Paolo Plateau off Brazil, as shown in Figure 9b. The numbers shown in Figure 13 lead to a value of $x_b = 24$ km—a value clearly less than $b = 446$ km. Thus again (3.1) is used to give a value of 16.3 Sv.

Hogg *et al.* (1982) report 4 ± 1.2 Sv based upon two years of current meter measurements and numerous dynamic sections. These are clearly the most accurate numbers to date for any sill flow, yet our large value of h_u raises the question of whether there is a shallower unmeasured flow leaning on the flanks of

Table 1 Data and predictions for four sills

Figure no.	*Sill*	$\frac{\Delta\rho}{\rho}$	h_u (*m*)	f (s^{-1})	b (*km*)	x_b (*km*)	Q (*Sv*)	$Q_{Observed}$ (*Sv*)	% *over*	*Citation*
10	Denmark Strait	3×10^{-4}	580	1.3×10^{-4}	350	14	3.9	2.5	1.6	Ross (1976)
11	Iceland–Faeroe	5.8×10^{-4}	400	1.3×10^{-4}	400	17	3.6	1.4	2.6	Steele *et al.* (1962)
12	Ceara Abyssal Plain	5×10^{-5}	430	1.0×10^{-5}	700	66	4.6	1.1–2.1	4.2–2.2	Whitehead & Worthington (1982)
13	Vema Channel	1×10^{-4}	1540	0.73×10^{-4}	446	24	16.3	4.0	4.1	Hogg *et al.* (1982)

the Sao Paolo Plateau. The fact that the estimates by this method are greater than the measurements is consistent with the notion that this method yields numbers that were greater than the actual flows.

Applying this simple approach to real ocean phenomena clearly has numerous weaknesses. In the first two examples, the sills were near the top surface and the assumption of a deep motionless layer of fluid above the flow is questionable. Fortunately, the need for the fluid to be deep is only required for time-dependent flows; a stationary flow only needs motionless (not deep) fluid above it. However, the real ocean violated these assumptions because the actual sill flow is time-dependent and there are other surface currents in the vicinity. Another problem is the location of the selected stations. The GEOSECS data set were used here and they are hardly optimal. In the Ceara Abyssal Plain, the southern (upstream) station was hundreds of kilometres from the sill, and the current must make its way over more than 500 km of flat abyssal plain. Surely friction will play a role there, the effective value of h_u clearly drops between the equator and 4 °N (Whitehead, 1989). Pratt (1986) also presented an estimate of friction parameters that indicate that friction can play a role in the Vema Channel, Denmark Strait, and the Iceland Faeroe Ridge. In the Vema Passage, our northern (downstream) station was even more poorly located and a closer station would have been desirable. Unfortunately, an exhaustive survey has not been conducted of all available data. However, it is clear that there is a large-scale trend to the north–south temperature field associated with the Antarctic region that extends up to 3000 m. That trend is responsible for the large value of h_u we selected, but it undoubtedly is associated with currents above the channel. Thirdly, role of stratification is neglected in this problem. Hogg (1983) constructed theories involving two and three dynamically active layers which certainly bear on the Vema Channel flow. Fourthly, there is no guarantee that the cross-section is the appropriate one for critical control. Pratt (1986) has found that friction may move the control point significantly downstream of the crest in a non-rotating problem. Our most questionable cross-section is the one adopted for the Vema passage, which possesses a sill depth of 4600 m whereas Hogg *et al.* (1982) considered a more southern section appropriate. We chose our section because our hydrographic data indicated a possible flow as shallow as 3000 m, and this section was the narrowest one with a wall on the left.

One must also remember that systematic errors sometimes exist in the ocean estimates due to temporal bias, faulty estimates of the level of no motion, errors in the actual width of the current, neglect of boundary layers, etc., thus the agreement is as good as could be expected. The estimates are 1.6 and 4.2 times the ocean estimates. This is the correct order of magnitude but of greater value, which is consistent with the concept that this is an upper bound. In the simplest conceptual sense, we have indicated that baroclinic density level differences between basins can be used to crudely estimate flux between the basin. In view of the numerous uncertainties, the agreement between a simple theory and ocean observations seems to indicate that the approach is promising.

4. LOCK-EXCHANGE FLOW AND APPLICATION TO SHALLOW SEAS

Lock-exchange flow is defined as the flow at the narrows and shallow region between basins with two different but uniform densities. In formulating problems, one visualizes a gate which, once removed, allows the set-up of a semi-steady exchange of flow and counterflow between the basins.

This problem, with rotation, was addressed with partial success by Whitehead *et al.* (1974). In that formulation, zero potential vorticity (which strictly requires very deep upstream basins) was used along with a somewhat contradicting energy conserving formula. Although laboratory data agreed with the theoretical prediction, a more complete theory would be useful, yet none has emerged.

The model consisted of two fluids of density difference lying in deep basins separated by a shallow channel of depth H_1. The flow and counter-flow are separated by a front of depth

$$h_2 = \frac{H_1}{2}\left[1 + \frac{x}{x_0}\right], \tag{4.1}$$

where

$$x_0 = \frac{\sqrt{g' H_1}}{2f}, \tag{4.2}$$

$$v_2 = v_1 - \sqrt{g' H_1} = \tfrac{1}{2}\sqrt{g' H_1}\left(1 - \frac{x}{x_0}\right), \tag{4.3}$$

$$Q = \tfrac{1}{2}\sqrt{g' H_1^{3/2}} L\left[1 - \frac{1}{3}\frac{L^2}{x_0^2}\right]. \tag{4.4}$$

This is only valid for channel width $L < x_0$. If $L > x_0$, the interface intersects the surface and the bottom of the sill, so

$$Q = \frac{1}{6}\frac{g' H_1^2}{f}. \tag{4.5}$$

5. APPLICATION TO SHALLOW SEAS

5.1 Spencer Gulf, South Australia

The lock-exchange formula was applied to the flow in Spencer Gulf, South Australia by Bye and Whitehead (1975). Using estimates for evaporation, budgets for conservation of water and salt were used in conjunction with (4.5) to predict the salinity difference between the gulf and the ocean.

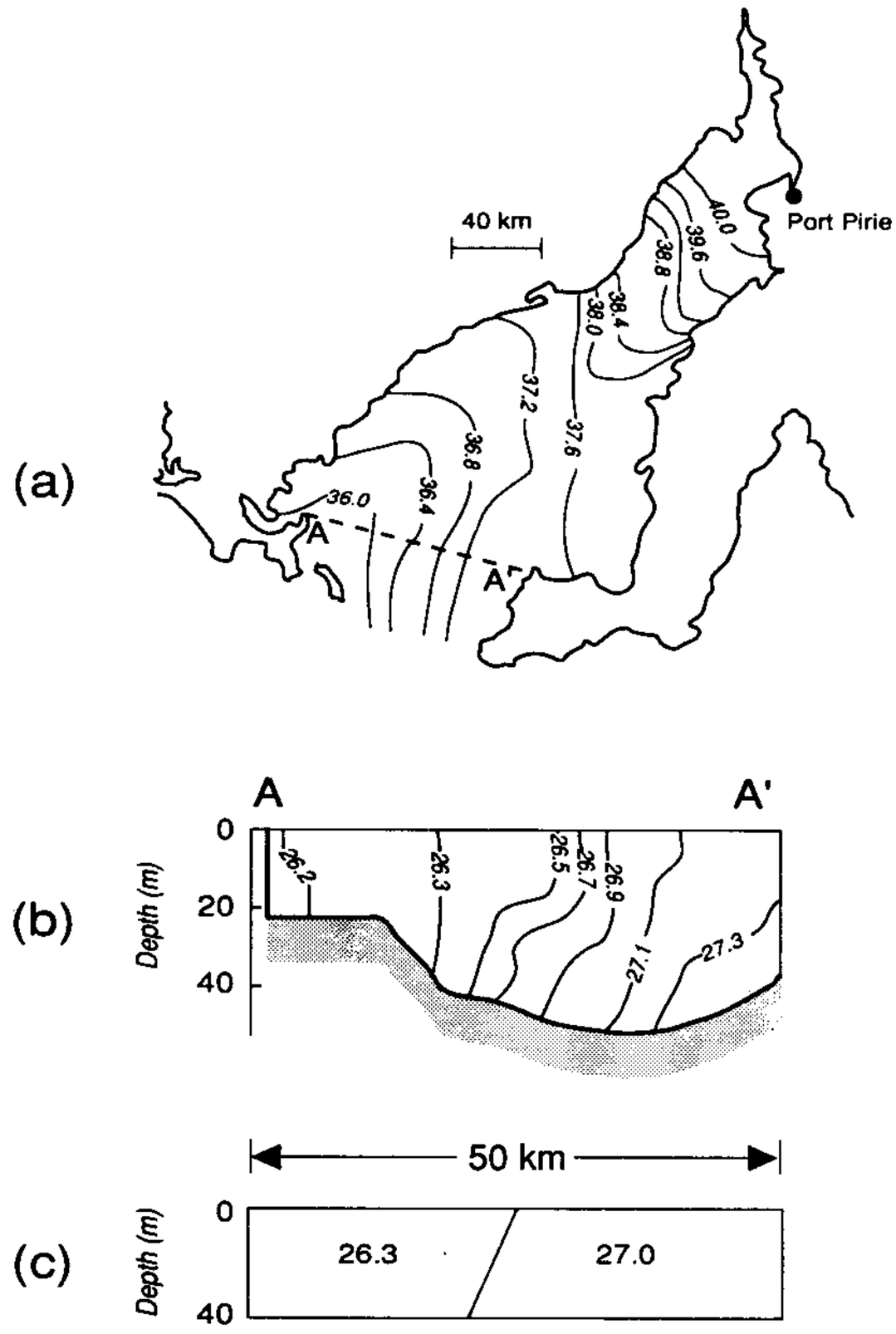

Figure 14 Front at the mouth of Spencer Gulf. (**a**) Plan view of surface salinity in Spencer Gulf. (**b**) Elevation view of density at the mouth of Spencer Gulf and (**c**) from the model. Note that not only does the density difference appear to agree crudely, but the tilt of the front across the mouth also seems to agree.

The volume and salt flux budgets through the mouth are

$$Q_o = Q_i + Q_e, \tag{5.1}$$

$$S_o Q_o = S_i Q_i, \tag{5.2}$$

where a subscript o denotes flow *out* of the gulf, i denotes *in*, and e denotes *evaporation*. Using $Q_e < Q_o$ or Q_i and $\Delta S < S_o$, we derive a relation for salinity difference

$$\Delta S = S_o - S_i = \frac{S_o Q_e}{Q_o}. \tag{5.3}$$

A dynamic relation between Q_o and ΔS was adopted from the lock-exchange formula (4.17).

$$Q_o = \frac{1}{6}\frac{g' H_1^2}{f}. \tag{5.4}$$

Using $g' = g\Delta\rho/\rho = g\beta\Delta S$, H_1 as the depth of the mouth of Spencer Gulf and f as the Coriolis parameter, a prediction of salinity difference as a function of Q_e and the other parameters was given as:

$$\Delta S = \left[\frac{6|f|SQ_e\rho}{g\beta H_1^2}\right]^{1/2}. \tag{5.5}$$

Using $\rho = 1.027\,\text{kg/l}$, $S = 35.9\,\text{ppt}$, $Q_e = 600\,\text{m}^3/\text{s}$, $f = -0.8\times10^{-4}\,\text{s}^{-1}$, $\beta = 0.71\times10^{-3}\,\text{kg/l ppt}$, $H_3 = 40\,\text{m}$ and $g = 9.8\,\text{m/s}^2$, we predicted $\Delta S = 0.98\,\text{ppt}$, which is equivalent to a density difference of $0.69\times10^{-3}\,\text{kg/l}$. Figure 14 shows an actual density distribution in comparison with the density difference and tilt predicted by this simple model and there is clearly rough agreement.

5.2 Chesapeake Bay, Eastern United States

Chesapeake Bay is located on the east coast of the United States. Its salinity is considerably less than the salinity of the ocean due to the influence of river runoff. Salinity of the bay is minimum at the extreme northern end, near the outflow of the Susquehanna River and increases gradually southward towards the mouth. At the mouth itself there is frequently a distinct front separating the fresher bay water from the ocean (shelf) water. We explore here the possibility that (5.5) with Q_e replaced by the volume flux of river runoff and salinity difference set to the opposite sign, is appropriate to predict the salinity difference across the front at the mouth of Chesapeake Bay. Boicourt (1973) reports a river runoff (principally from the Susquehanna River) of $2237\,\text{m}^3/\text{s}$. Using this in Eq. (5.5) with $H = 10\,\text{m}$, $f = 0.88\times10^{-4}\,\text{s}^{-1}$, $S = 30\,\text{ppt}$ with the above values of g and b gives

$$\Delta S = 7.2‰. \tag{5.6}$$

This gives a tilted front span $2x_0 = 8.0\,\text{km}$. Figure 15a shows the surface salinity distribution near the mouth from a survey by Blume *et al.* (1977). The shape of the front is consistent with bay water flowing seaward along the southern shore of the mouth region, oceanic water flowing bayward along the northern shore and a clear front between. A salinity jump of six to eight parts per thousand is the approximate amplitude across the front. Although more data are not shown here, this is a typical picture of the front. It usually extends from the water surface to the bottom of the bay, although over a deep blind channel the fresh water often detaches from the bottom (Figure 15b). The model predictions for ΔS and x_0 are

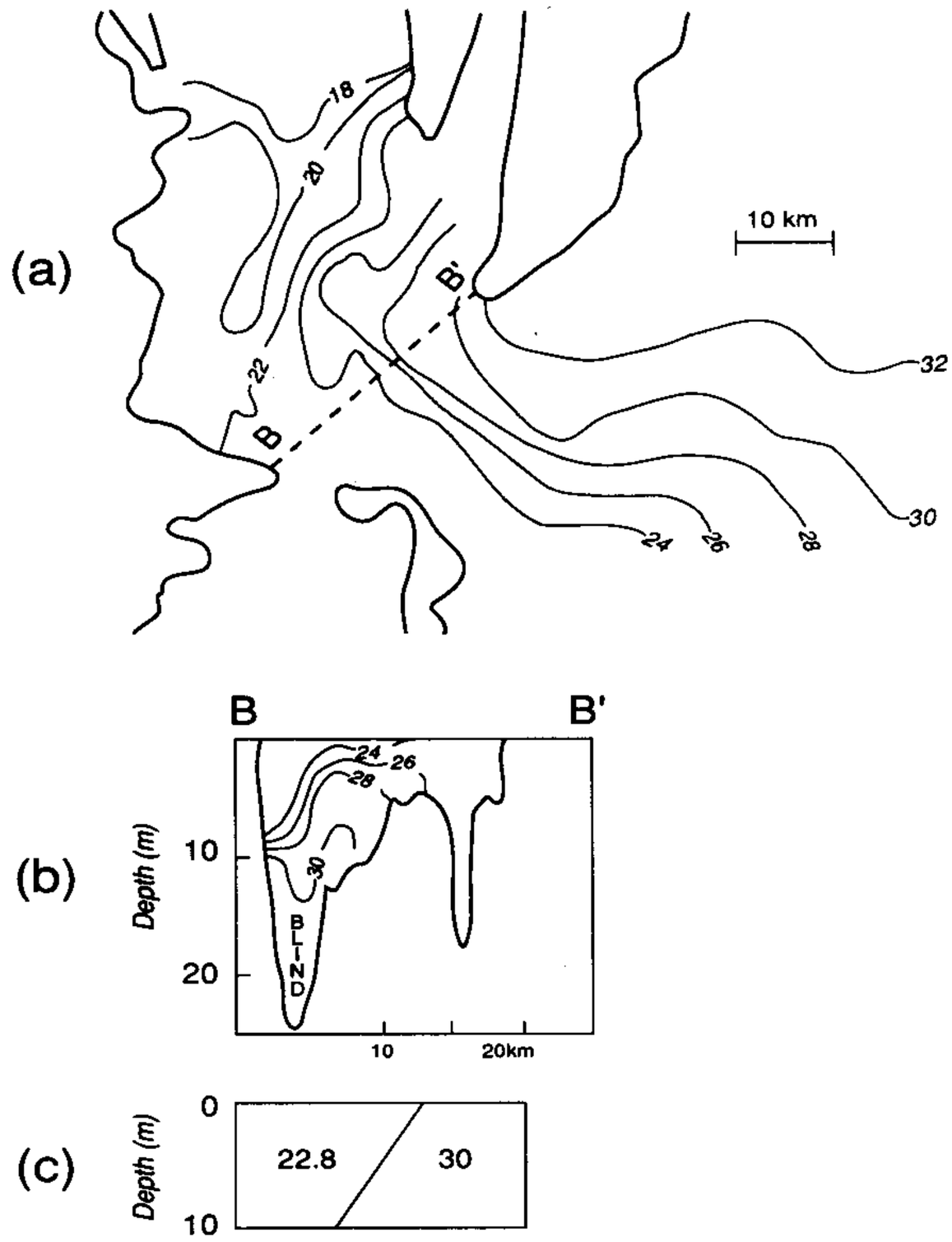

Figure 15 Front at the mouth of Chesapeake Bay. (**a**) Plan view of surface salinity in the vicinity of the mouth of Chesapeake Bay on 24 August 1976. (**b**) Elevation view of the salinity distribution at the mouth. (**c**) Results of the model predictions.

sketched in Figure 15c. Thus the results crudely resemble the bay. In spite of this being a "typical" picture, the actual front exhibits considerable variability during large wind events and after extreme rainstorms. Moreover, other causes for the structure have been proposed, the two most notable being a shoaling of the bathymetry in the northern part of the mouth and the fact that some rivers flow into the southern regions near the mouth. We can only propose this as a possible effect—a dynamic rotating salt wedge—that contributes to the ecological climate of the bay.

5.3 Other Seas

The Strait of Gibraltar consists of flow and counterflow driven by the excess salinity of the waters of the Mediterranean Sea compared to the Atlantic. The appropriate parameters revealed that the small rotation limit (4.4) was appropriate and that volume flux would be less than 10% different from the classical non-rotating result. However, recently Miyake *et al.* (1988) reported an outflow of

dense water from Funka Bay in Hokkaido, Japan that appears to fit the rapid rotating limit well. The sill depth is 80 m, the width of the mouth is 14 nautical miles and the width of the current [$2x_0$ using (4.2)] was calculated to be 2.6 nautical miles. The actual width of the current was approximately 3 nautical miles.

6. SUMMARY

The simple hydraulics formulation appears to give reasonable quantitative agreement to a variety of ocean problems. We are not aware that such dynamics have yet been incorporated in ocean numerical circulation models which raises the question of how deep water below approximately 4000 m travels from one basin to the next, and how bottom temperature is determined.

The agreement of the applications of the formulas with ocean measurements suggests that the inertial acceleration of water due to density differences between water basins may be an important component in ocean circulation between basins. It is clear that rotation of the earth can be successfully incorporated, although in all cases the equations are nonlinear and exact solutions will probably only be found for idealized circumstances. One finds crude agreement in a variety of settings. The calculations are reasonably simple and without adjustable constraints or unknown constants such as "eddy mixing", but complexity and difficulty increases rapidly as more "ocean reality" is put into the problem.

Pratt (1986) presented estimates of parameters that indicate that friction is significant in such ocean passages. The calculations here indicate that friction will probably decrease volume flux by only a factor of four or less compared to inviscid estimates. Unfortunately, the true role of friction is not understood in either rotating hydraulic problems or in critically controlled stratified flows.

Precise calculations are possible with computers and more ocean measurements could be undertaken. Both involve considerable expense. Such approaches may well be warranted for various reasons, and the tools described in this paper may fruitfully be used for the first approximation.

Acknowledgments

Support is gratefully acknowledged from the Office of Naval Research, Division 1121CS, Contract No. 00014-87-K-0003 NR083-004. Anne-Marie Michael patiently typed numerous drafts of this manuscript.

References

Beardsley, R. C. and Festa, J. C., "A numerical model of convection driven by a surface stress and non-uniform horizontal heating", *J. Phys. Ocean.* **2**, 444–455 (1972).

Blume, H.-J. C., Kendall, B. M. and Fedors, J. C. *Sea Surface Temperature and Salinity Mapping from Remote Microwave Radiometric Measurements of Brightness Temperatures.* NASA Technical Paper, 1077, National Technical Information Service, Springfield, VA 22161 (1977).

Boicourt, W. C., *The Circulation of Water on the Continental Shelf from Chesapeake Bay to Cape Hatteras*, Ph.D. Dissertation, Johns Hopkins University, Baltimore, Maryland (1973).

Bye, J. A. T. and Whitehead, J. A., "A theoretical model of the flow in the Mouth of Spencer Gulf, South Australia", *Est. Coast. Mar. Sci.* **3,** 477–481 (1975).

Dietrich, G., "Schichtung und Zirkulation der Irnminger—See Im Juni 1955", *Beidt. Wiss. Kommn. Meeres-forsch* **14,** 255–312 (1957).

Eggvinn, J. H. K. and Lygren, S., *Bathymetric Chart of the Norwegian Sea and Adjacent Areas,* Fiskeridirektoratets Havforskningsinstitutt, Norway (1963).

GEOSECS Atlantic Expedition. Volume 1: Hydrographic Data; and Volume 2: Sections and Profiles. U.S. Government Printing Office, Washington, D.C.

Gill, A. E., "The hydraulics of rotating channel flow", *J. Fluid Mech.* **80,** 614–670 (1977).

Hogg, N. G., "Hydraulic control and flow separation in a multi-layered fluid with applications to the Vema Channel", *J. Phy. Ocean.* **13,** 695–708 (1983).

Hogg, N. G., Biscaye, P., Gardner, W. and Schmitz, W. J. Jr., "On the transport and modification of Antarctic Bottom Water in the Vema Channel", *J. Mar. Res.*, Suppl. to **40,** 231–263 (1982).

Miyake, H., Tanaka, I. and Murakami, T., "Outflow of water from Funka Bay, Hokkaidǫ, during early spring", *J. Ocean. Soc. Japan* **44,** 163–170 (1988).

Moody, R., Hayes, D. E. and Connary, S., *Bathymetry of the Continental Margin of Brazil,* Map number 832, *Am. Ass. Petroleum Geol.*, Tulsa, Oklahoma (1979).

Pratt, L. J., "Hydraulic control of sill flow with bottom friction", *J. Phys. Ocean.* **16,** 1970–1980 (1986).

Pratt, L. J. and Armi, L., "Hydraulic control of flows with non-uniform potential vorticity", *J. Phys. Ocean.* **17,** 2016–2029 (1987).

Ross, C. K., *Overflow 73—Transport of Overflow Water through Denmark Strait.* International Council for the Exploration of the Sea. C.M. C:16, unpublished manuscript (1976).

Rossby, H. T., "On thermal convection driven by non-uniform heating from below: An experimental study", *Deep-Sea Res.* **12,** 9–16 (1965).

Shen, C. Y., "The rotating hydraulics of the open-channel flow between two basins", *J. Fluid Mech.* **112,** 161–188 (1981).

Speer, K. G. and Whitehead, J. A., "A gyre in a non-uniformly heated rotating fluid", *Deep-Sea Res.* **35,** 1069–1077 (1988).

Steele, J. H., Barrett, J. R. and Worthington, L. V. "Deep currents south of Iceland", *Deep-Sea Res.* **9,** 465–474 (1962).

Stommel, H., "On the smallness of sinking regions in the ocean", *Proc. Nat. Acad. Sci.* **48,** 776–772 (1962).

Whitehead, J. A., "Surges of Antarctic Bottom Water into the North Atlantic", *J. Phys. Ocean.*, in press (1989).

Whitehead, J. A., Leetmaa, A. and Knox, R. A., "Rotating hydraulics of strait and sill flows", *Geophys. Fluid Dynam.* **6,** 101–125 (1974).

Whitehead, J. A. and Worthington, L. V., "The flux and mixing rates of Antarctic Bottom Water within the North Atlantic". *J. Geophys. Res.* **87,** 7903–7924 (1982).

Worthington, L. V., "An attempt to measure the volume transport of Norwegian Sea overflow water through the Denmark Strait", *Deep-Sea Res.* **16,** 421–432 (1969).